ADVANCED MATERIALS
www.advmat.de

Piezotronic Tunneling Junction Gated by Mechanical Stimuli

Shuhai Liu, Longfei Wang, Xiaolong Feng, Jinmei Liu, Yong Qin, and Zhong Lin Wang**

Tunneling junction is used in many devices such as high-frequency oscillators, nonvolatile memories, and magnetic field sensors. In these devices, modulation on the barrier width and/or height is usually realized by electric field or magnetic field. Here, a new piezotronic tunneling junction (PTJ) principle, in which the quantum tunneling is controlled/tuned by externally applied mechanical stimuli, is proposed. In these metal/insulator/piezoelectric semiconductor PTJs, such as Pt/Al_2O_3/*p*-GaN, the height and the width of the tunneling barriers can be mechanically modulated via the piezotronic effect. The tunneling current characteristics of PTJs exhibit critical behavior as a function of external mechanical stimuli, which results in high sensitivity (≈5.59 mV MPa^{-1}), giant switching (>10^5), and fast response (≈4.38 ms). Moreover, the mechanical controlling of tunneling transport in PTJs with various thickness of Al_2O_3 is systematically investigated. The high performance observed with these metal/insulator/piezoelectric semiconductor PTJs suggest their great potential in electromechanical technology. This study not only demonstrates dynamic mechanical controlling of quantum tunneling, but also paves a way for adaptive interaction between quantum tunneling and mechanical stimuli, with potential applications in the field of ultrasensitive press sensor, human–machine interface, and artificial intelligence.

According to quantum mechanics, carriers have a probability of tunneling through a barrier as long as the barrier is sufficiently thin.[1] The transmittance depends exponentially on the barrier profile and the available carrier states,[1,2] which makes a tunneling junction possess a giant switching of tunneling resistance. Meanwhile, the tunneling time is governed by the reciprocation of transition probability per unit time, which is much shorter than the conventional transit time.[2,3] Due to these inherent advantages over other types of junctions, devices based on quantum tunneling generally exhibit both merits of high switching and fast response. Esaki diode,[4] superconductor Josephson junction,[5] magnetic tunneling junction,[6] and most recently ferroelectric tunneling junction[7–9] are well-known examples that have attracted much attention. Up to now, numerous works are focused on direct use of electric field or magnetic field to modify the barrier profile and the carrier states, so as to control the tunneling transport.[10–16] The regulating mechanism inspires much promise for electronic applications as varied as high-frequency oscillators,[17,18] nonvolatile memories,[19–21] and magnetic field sensors.[22] However, there are few reports of tunneling junction gated by external mechanical stimuli that are ubiquitous and abundant in environment, which is very important for developing quantum mechanics. Therefore, it is highly desired to find schemes for developing mechanically tunable tunneling junctions.

A coupling of piezoelectricity and electronic transport processes in piezoelectric semiconductor materials under mechanical stimuli results in an emerging field of piezotronics,[23–26] which use the inner crystal potential generated by the strain-induced remnant piezoelectric polarization charges as a "gate" controlling signal to redistribute the free carriers and thus modify the energy profile, so as to control the electronic transport at interface/junction.[27–30] This mechanism has demonstrated its effectiveness and high performance in junctions with finite height, including the Schottky junction and *p*-*n* junction,[31–33] and triggered a variety of electromechanical applications including logic unit,[34]

Dr. S. H. Liu, Dr. J. M. Liu
School of Advanced Materials and Nanotechnology
Xidian University
Xi'an, Shaanxi 710071, China
Dr. L. F. Wang, Prof. Z. L. Wang
Beijing Institute of Nanoenergy and Nanosystems
Chinese Academy of Sciences
Beijing 100083, China
E-mail: zhong.wang@mse.gatech.edu
Dr. L. F. Wang, Prof. Z. L. Wang
College of Nanoscience and Technology
University of Chinese Academy of Sciences
Beijing 100049, China
Dr. L. F. Wang, Prof. Z. L. Wang
School of Material Science and Engineering
Georgia Institute of Technology
Atlanta, GA 30332, USA
Dr. X. L. Feng
Research Laboratory for Quantum Materials
Singapore University of Technology and Design
Singapore 487372, Singapore
Prof. Y. Qin
Institute of Nanoscience and Nanotechnology
School of Physical Science and Technology
Lanzhou University
Lanzhou, Gansu 730000, China
E-mail: qinyong@lzu.edu.cn

The ORCID identification number(s) for the author(s) of this article can be found under https://doi.org/10.1002/adma.201905436.

DOI: 10.1002/adma.201905436

tactile imaging,[35] and electronic skin.[36] This approach of utilizing mechanical stimuli to engineering energy-band, together with its high performance, is fundamentally new in science and theoretically feasible for mechanically tunable quantum tunneling.

Here, we propose a novel piezotronic tunneling junction (PTJ) with metal/insulator/piezoelectric semiconductor heterostructure. In these PTJs, both the height and the width of the tunneling barrier are first modulated by the external mechanical stimuli as a result of the piezotronic effect, and then, this continuous modification of Schottky barrier makes a notable modulation of the dividing voltage on insulator and hence the tunneling transport. A real PTJ with Pt/Al_2O_3/*p*-GaN heterostructure is rationally designed and successfully developed. The tunneling current of the PTJ exhibits the critical behavior characteristic as a function of external stimuli, in which the sensitivity is up to ≈5.59 mV MPa^{-1}, the ON/OFF conductance ratio is above 10^5, and the time response is ≈4.38 ms. Moreover, the mechanical control of tunneling transport in PTJs with various Al_2O_3 thickness from 0.95 to 4.78 nm is systematically investigated. This study demonstrates high sensitivity, giant switching, and fast response of the metal/insulator/piezoelectric semiconductor PTJs, which not only provides an in-depth understanding about the piezotronic effect on quantum tunneling but also proves their great potential in adaptive interaction between quantum tunneling and mechanical stimuli.

To realize the piezotronic tunneling junction gating by mechanical stimuli, we designed a structure of Pt/Al_2O_3/*p*-GaN by replacing one metal electrode with a piezoelectric semiconductor and systematically investigated its working mechanism by means of theoretical simulation. As depicted schematically in **Figure 1**a, if the interfacial layer (Al_2O_3) is sufficiently thin, charge will leak through the barrier to establish thermal equilibrium as a single system.[1,2] As a result, the semiconductor surface will be depleted of majority carriers within a finite width.[2] And an abrupt discontinuity in energy profile, formed by a series connection of an insulating barrier and a Schottky barrier, will exist between Pt and *p*-GaN. This discontinuity of energy-band is responsible for controlling the current conduction as well as its capacitance behavior.[2] The tunneling electrons have to experience an extra barrier over the space charge region because the semiconductor surface is depleted. In this case, the Pt/Al_2O_3/*p*-GaN tunneling junction is set to a high resistance OFF state. As wurtzite structured III-nitride semiconductor, GaN possesses both piezoelectric (Figure S1, Supporting Information) and semiconductor properties. Owing to the piezoelectric effect along the *c*-axis (d_{33}) and to the incomplete screening of polarization by free charges,[26] upon straining along the *c*-axis [0001], negative polarization charges along the *c*-axis induced at the Al_2O_3/*p*-GaN interface can drive the p-type semiconductor surface out of depletion and reduce the barriers' height and width via piezotronic effect (Figure 1b). This critical modification of barrier profile will make a notable

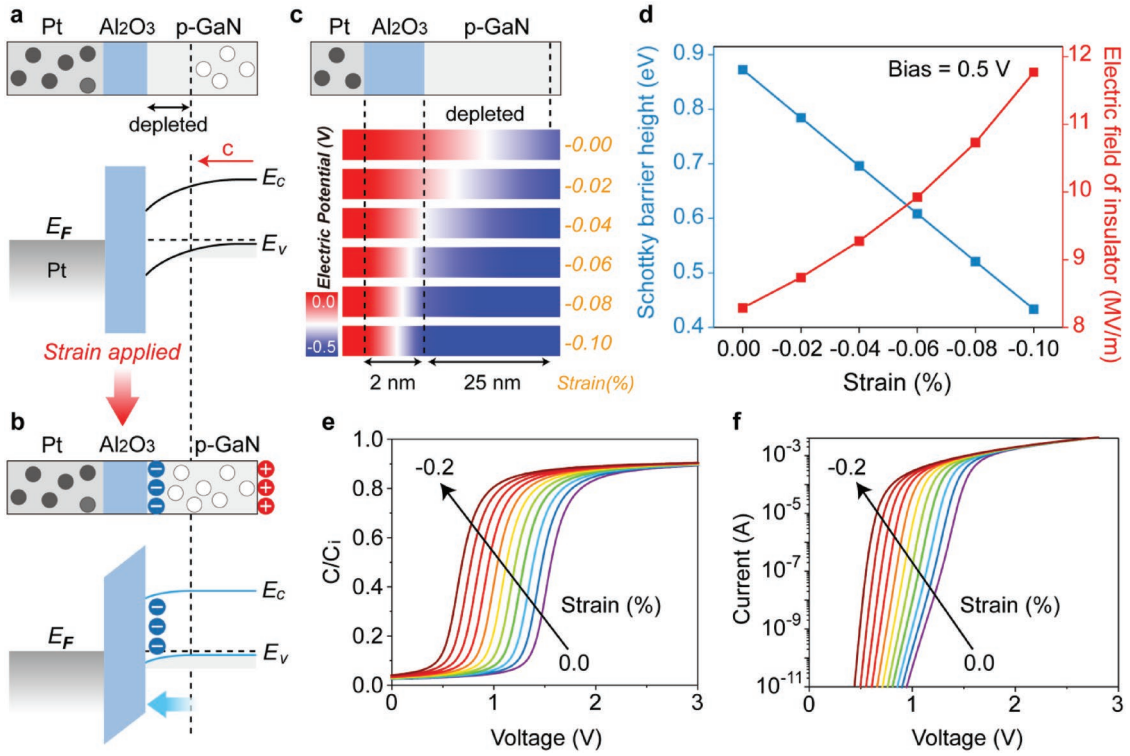

Figure 1. Working mechanism of mechanically controlling/tuning of quantum tunneling via the piezotronic effect. Band diagram of Pt/Al_2O_3/*p*-GaN heterostructure under a) strain free and b) strain conditions. c) Calculated potential distribution of the tunneling junction under strain along the *c*-axis. The potentials of Pt and *p*-GaN are biased to be 0 and 0.5 V, respectively. d) The Schottky barrier height and the electric field of insulator as a function of externally applied strains. Calculated e) *C*–*V* and f) *I*–*V* characteristics of the tunneling junction under various strains. C_i and *C* present the insulator capacitance and the total capacitance of junction, respectively.

incensement of the dividing voltage and the corresponding electric field in the insulator. As simulated in Figure 1c,d, the barrier's height and the depletion width both gradually decrease, while the insulating electric field gradually increases as the strain increases. In contrast to the OFF state, the tunneling transmittance can be greatly improved by external mechanical stimuli. The tunneling junction is then set to a low resistance ON state. As calculated in Figure 1e,f, the *C*–*V* and the *I*–*V* characteristics are both continuously increased with applied strain from 0.0% to −0.2%. Therefore, through exploiting dynamic mechanical controlling of quantum tunneling by piezotronic effect, we can theoretically implement a mechanically tuned tunneling junction with metal/insulator/piezoelectric semiconductor heterostructure.

To verify the above theoretical analysis, we designed a set of comparison experiments. The Al_2O_3/*p*-GaN heterostructure is fabricated by depositing Al_2O_3 on *p*-GaN single crystal films using atomic layer deposition (ALD, Figure S2, Supporting Information). In this work, we use a Pt/Ir-coated tip to apply compressive forces and simultaneously measure the tunneling current through conductive atomic force microscope (c-AFM) (**Figure 2**a). The normalized background noises of current characterization are lower than ±10 and ±30 pA in 10 nA and 10 µA measurement range, respectively (Figure S3, Supporting Information). The AFM tip with a diameter of about 50 nm (Figure S4, Supporting Information) was first engaged on the facet vertical to the *c*-axis [0001] of *p*-GaN. Being subjected to the external mechanical stimuli, the *p*-GaN experiences a *c*-axial strain and produces negative piezoelectric charges on its surfaces within a thickness of one to two atomic layers,[37] as indicated in Figure 2a. The negative piezopotential created at the Al_2O_3/*p*-GaN interface not only lowers the barrier height but also reduces the depletion width. This modification of energy profile will increase the insulator electric field and improve

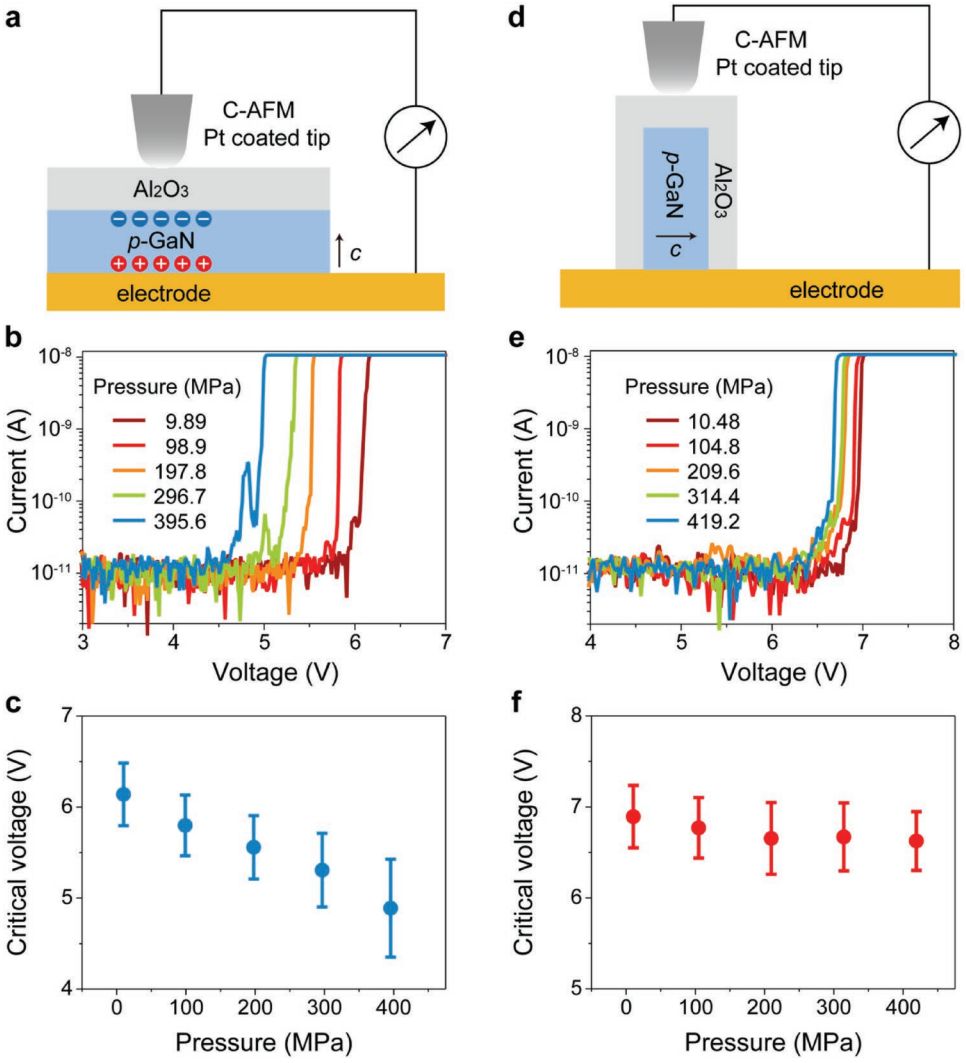

Figure 2. Tunable critical voltage of tunneling junction upon straining along the *c*-axis and the *m*-axis of *p*-GaN. a) Schematic of Pt/Al_2O_3/*p*-GaN tunneling junction along the *c*-axis of *p*-GaN. b) The corresponding *I*–*V* characteristics upon the applied pressures. c) The tunable critical voltage V_c as a function of the applied pressures along the *c*-axis. d) Schematic of Pt/Al_2O_3/*p*-GaN tunneling junction along the *m*-axis of *p*-GaN. e) The corresponding *I*–*V* characteristics upon the applied pressures. f) The tunable critical voltage V_c as a function of the applied pressures along the *m*-axis. The Al_2O_3 thickness is about 1.91 nm.

the tunneling current. The mechanical modulation process of the quantum tunneling is showed intuitively in Figure S5 (Supporting Information). As performed in Figure 2b, when the pressure is increased from 9.89 to 395.6 MPa, the critical voltage gradually decreases, which is consistent with the above theoretical calculations (Figure 1f). In order to determine this regulatory relationship more accurately, we performed statistics on about 300 times of measurements (Al_2O_3 thickness ≈1.91 nm, Figure S6, Supporting Information) and plotted the critical voltage as a function of applied force showing in Figure 2c, which suggest a strong correlation between them within a certain range of force (0–400 MPa). In this force range, we have not observed surface damage (Figure S7, Supporting Information).

To further demonstrate the piezotronic effect on quantum tunneling, we characterized the tunneling transport by applying a force on a nonpolarization surface (*m*-axis [$1\bar{1}00$]) of the same *p*-GaN wafer by rotating 90°, as shown in Figure 2d. In this case, there will be no piezoelectric polarization charges induced at the Al_2O_3/*p*-GaN interface due to the crystallographic symmetry of GaN (Figure S1, Supporting Information). The critical voltage is only slightly fluctuated within a small range, which may be mainly due to the increased contact area between the tip and the Al_2O_3 layer (Figure 2e). Correspondingly, the statistic of critical voltage with error bar derived from about 230 times of measurements is plotted as a function of applied compressive force (Figure 2f; Figure S8, Supporting Information). There is almost no obvious correlation between the critical voltage and the applied pressures, compared to the case when the strain is applied along the *c*-axis of *p*-GaN. The difference can confirm the critical role of the piezotronic effect on the mechanical controlling of quantum tunneling.

To give an in-depth understanding about the working mechanism of the piezotronic effect on quantum tunneling, we systematically investigate the PTJs with various insulating barrier thicknesses (**Figure 3** and Note S1, Supporting Information). Figure 3a depicts band alignments of tunneling junctions with different Al_2O_3 thicknesses. The strain-induced negative piezoelectric bound charges at the Al_2O_3/*p*-GaN interface can attract majority carriers to move toward the semiconductor surface and lower the barrier's height and width via piezotronic effect. This profile modification of energy band redistributes the potential drops across the PTJ and improves the electric field inside the insulator layer. As the insulator thickness increased, the change of electric field in the insulating layer is smaller. Figure 3b shows the ratio of electric field in insulating layer with various thicknesses under strain and strain-free conditions. The value decreases rapidly as the insulator thickness increases, especially within six nanometers, indicating that the modulation effect on the tunneling junction will become weaker. In order to prove this theory, we performed statistics on about 300 times of measurements of PTJs with various insulator thicknesses from 0.95 to 4.78 nm (Figure S6, Supporting Information). The normal distribution fitting curves are plotted in Figure 3c,

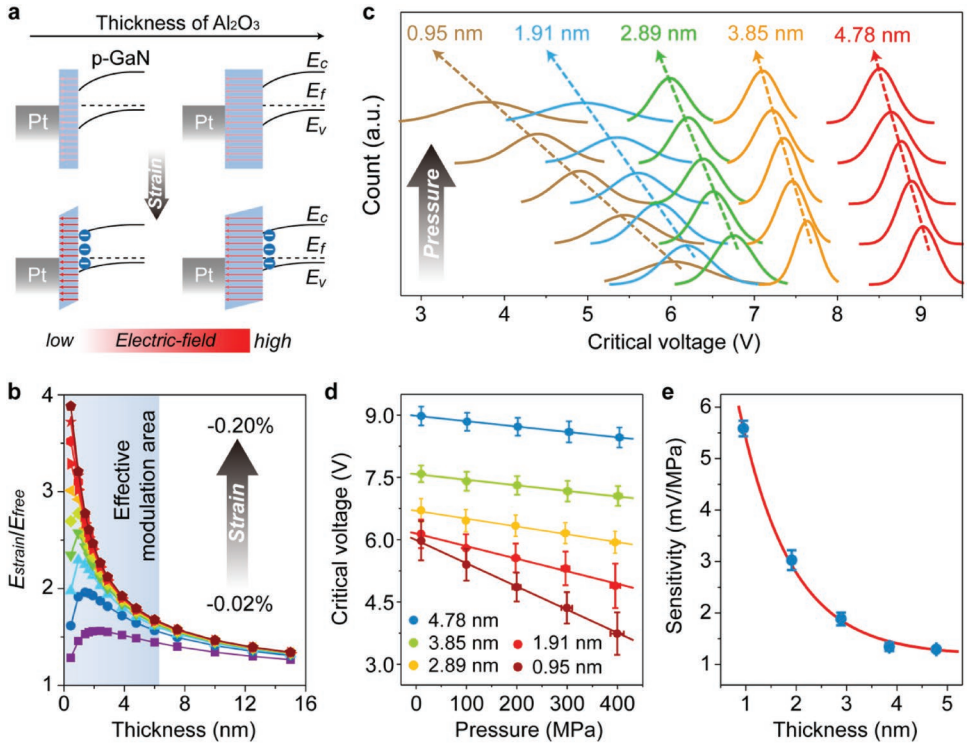

Figure 3. Piezotronic tunneling junction with various insulator thicknesses. a) Band diagrams of tunneling junctions with various insulator thicknesses to explain the piezotronic effect modulation. The colored arrows indicate the electric field strength in the insulator. b) Calculated thickness dependence of E_{strain}/E_{free} under various strains. E_{strain} and E_{free} represent the electric field of insulator under strain and strain-free conditions, respectively. c) Normal distribution of experimentally measured critical voltage V_c with various Al_2O_3 thicknesses. d) Critical voltage V_c of tunneling junction with various Al_2O_3 thicknesses as a function of the applied pressures. e) Pressure sensitivity versus the Al_2O_3 thickness.

which suggests that the modulation effect is more significant when the Al_2O_3 thickness decreases. The statistic critical voltage as a function of the applied pressures with various insulator thicknesses is plotted and found to have an approximate linear relationship with the applied pressure (Figure 3d). In order to quantitatively characterize the thickness dependence of mechanical controlling of tunneling transport, a pressure sensitivity is defined as the change of critical voltage per unit pressure: $(V_{force} - V_{free})/\Delta P$, where V_{force} and V_{free} correspond to the changes of critical voltage under pressure and pressure-free conditions, respectively, and P denotes the applied pressure. The pressure sensitivity as a function of Al_2O_3 thickness is shown in Figure 3e, which exhibits a higher sensitivity with decreasing insulating thickness, and is consistent with above theoretical simulation. The highest sensitivity of ≈5.59 mV MPa^{-1} is achieved in PTJ with 0.95 nm thickness of Al_2O_3.

The tactile imaging based on the PTJ is tested using an AFM system in tapping scanning mode to explore the switching performance. The thickness of the insulator layer we adopted in the junction is about 0.95 nm. The force imaging measurement was performed via applying various normal forces with well-determined values at different zones that form a force distribution image as a whole. We alternately applied small force (≈18 nN, ≈9 MPa) and large force (≈370 nN, ≈188 MPa) to achieve quantum tunneling off state and on state at a fixed bias of 5.3 V (**Figure 4**a). The small force of ≈18 nN is to ensure a good conductive contact but without triggering the tunneling effect. The large force of ≈370 nN is used to control the quantum tunneling while not destroying the insulator surface during 2D mechanical scanning process, which is also confirmed by the force mapping measurement (Figure S9, Supporting Information). As can be seen from the current response mapping in Figure 4a and Figure S10 (Supporting Information), the contours of the different force regions are distinguished very well, which demonstrates the great potential of mechanically tunable tunneling junctions for tactile imaging. The on and off resistance values and the corresponding on/off ratios of the dotted lines marked in Figure 4a are shown in Figure 4b,c. The on/off ratio has an average value of about 1.34×10^5 and its logarithmic value presents the normal distribution (Figure S11, Supporting Information), which indicates the giant switching and good regional consistency of $Pt/Al_2O_3/p$-GaN PTJs. By using the Young's modulus of GaN (≈352 GPa),[38] we can roughly estimate the strain of GaN under 9 and 188 MPa to be about –0.003% and –0.053%, respectively. The gauge factor (GF = $(\Delta I/I_0)/\varepsilon$, where ε is the strain) of this piezotronic tunneling junction can be qualitatively estimated to be about 2.6×10^8, which is a high value among the existing devices based on piezotronic or piezoresistive effect in Table S1 (Supporting Information). However, it should be noted that since the probe tip is not an ideal platform, the actual gauge factor should be a little less than the estimated value here.

The response time is another important factor for the tactile sensors. In order to accurately estimate the response time of PTJs to dynamic mechanical stimuli, we define a statistical value, describing the degree of quantum tunneling activation: active pixel percentage η. The value is calculated by the ratio: N_{actual}/N_{theory}, where N_{actual} and N_{theory} correspond to the number of pixels actually and theoretically activated, respectively.

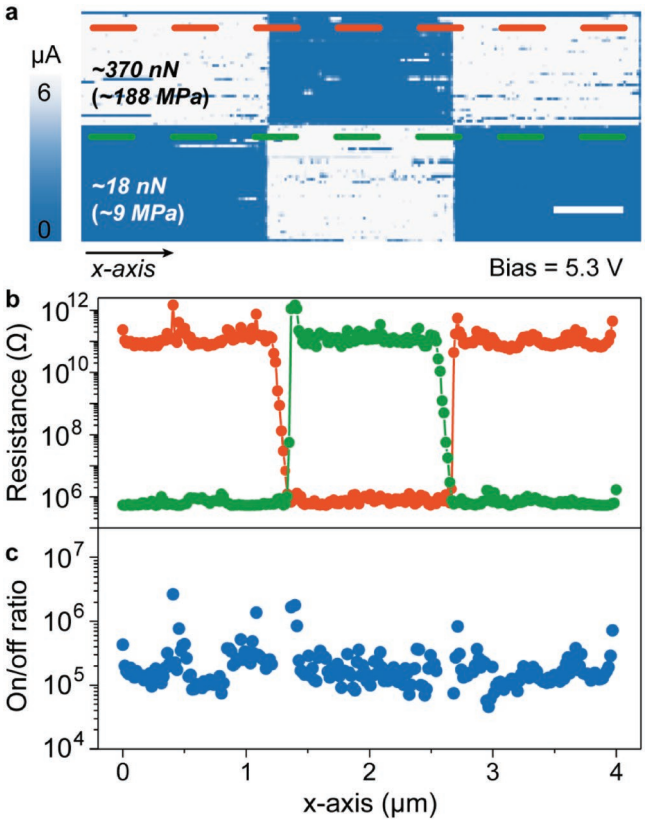

Figure 4. Tactile imaging based on PTJ. a) Current response contour plot by c-AFM demonstrating the capability of mechanically tunable tunneling junction for imaging the spatial profile of applied force/pressure. The scale bar is 1 μm. The Al_2O_3 thickness is about 0.95 nm. The b) resistances and the corresponding c) on/off ratios derived from the dotted lines in (a).

As exhibited in **Figure 5**a,b and Figures S12 and S13 (Supporting Information), we are able to obtain the current response for imaging the spatial profile "NANO" of applied forces with various pixel sizes and scan speeds. The current response profile is more obvious as the pixel size increases and more stable as the scanning speed decreases. By deriving η from these data, we obtain the relationship between the active pixel percentage with the pixel size and the scan speed (Figure 5c,d). By increasing the pixel size or reducing the scan speed, the active pixel percentage can be effectively improved. Furthermore, by converting the two parameters to contacting time, the active pixel percentage versus contacting time can be easily plotted in Figure 5e. A constant time of approximately 4.38 ms is calculated by nonlinear fitting, which is much less than that of human fingertips (≈30–50 ms) and can be further improved in future designs. These results indicate that the PTJ can respond quickly to statics as well as dynamic mechanical stimuli.

In summary, we successfully developed a new principle of piezotronic tunneling junction with the $Pt/Al_2O_3/p$-GaN heterostructure that can be gated by external mechanical stimuli via the piezotronic effect. It utilizes the strain-induced piezoelectric polarization charges to modulate the height and width of tunneling barriers, thereby realizing the modulation of the potential drop and electric field of the insulator layer, and

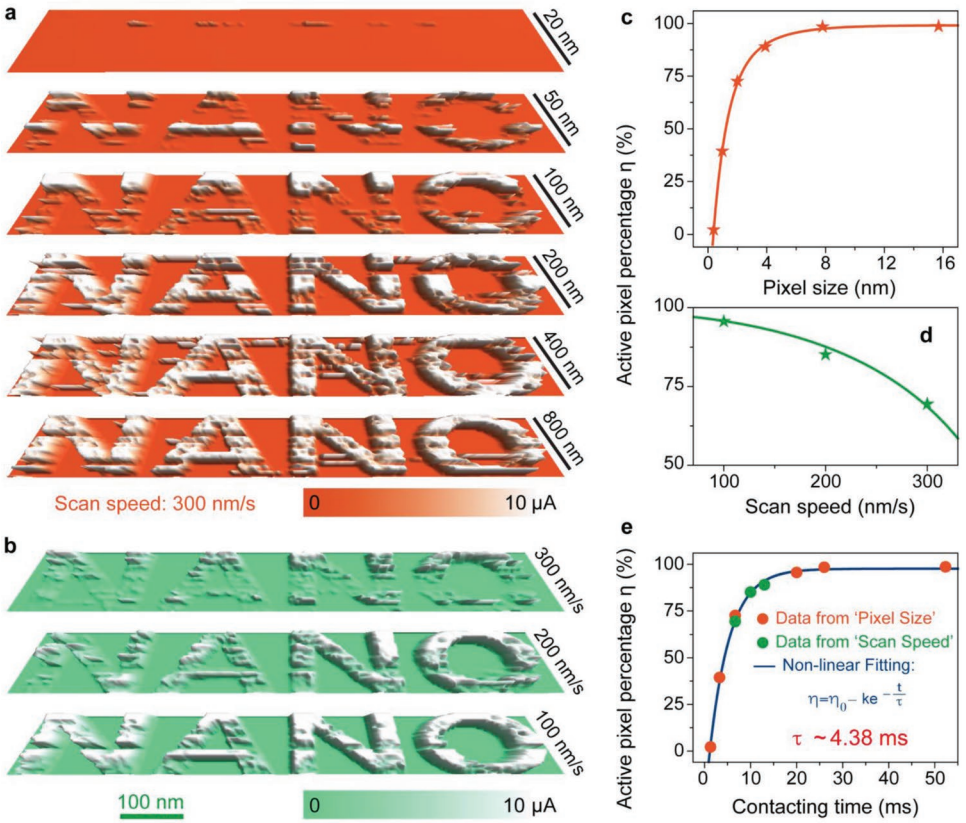

Figure 5. 3D current response of tactile imaging. 3D current response contour plot for imaging the spatial profile "NANO" of applied force with various a) pixel sizes and b) scan speeds. The Al_2O_3 thickness is about 0.95 nm. Active pixel percentage η as a function of c) pixel size and d) scan speed, derived from the tactile imaging in (a) and (b), respectively. The active pixel percentage η presents the percentage of pixels that are actually turned "on" when "on" input force signal is applied. e) Active pixel percentage η versus the contacting time calculated from (c) and (d). The solid line corresponds to the nonlinear fitting.

finally achieving the mechanical control of tunneling transport. The PTJs can respond to static as well as dynamic mechanical stimuli, which present high sensitivity (≈5.59 mV MPa^{-1}), giant switching (≈1.34 × 10^5), and fast response (≈4.38 ms). This study shows the effectiveness of piezotronic effect on tunneling junction and, all together with the high performance, suggests their great potential in adaptive interaction between quantum tunneling and mechanical stimuli.

Experimental Section

GaN Film: The [0001]-oriented single crystal GaN film was purchased from Suzhou Nanowin Science and Technology Co., Ltd., which was synthesized on the *c*-plane polished sapphire substrate by metalorganic chemical vapor deposition. The specific parameters of *p*-GaN films (provided by Suzhou Nanowin Science and Technology Co., Ltd.) were as follows, dimensions: Φ 50.8 mm ± 0.1 mm; thickness: ≈5 μm; orientation: *c*-plane (0001) ± 0.5°; conduction type: p-type (Mg-doped); resistivity (300 K): ≈10 Ω cm; carrier concentration: ≈6 × 10^{16} cm^{-3}; dislocation density: < 5 × 10^8 cm^{-2}; substrate structure: GaN on sapphire (Standard: SSP Option: DSP).

Piezoresponse Measurement: The piezoresponse on the *c*-plane and *m*-plane GaN was performed using AFM (Cypher ES, Asylum Research) with PFM (piezoresponse force microscopy) mode. The conductive tips of Pt/Ir coating, with a spring constant of about 2.8 nN nm^{-1} and a radius of about 25 nm, were used in PFM mode. The resonance frequency was ≈380 kHz for PFM mode. The dual AC resonance tracking (DART) mappings with AC drive voltages ranged from 0.5 to 1.5 V were implemented to measure the effective piezoelectric coefficient d_{33} (Figure S1, Supporting Information). Also, the tip voltages swiped from −6 to 6 V were applied to study the amplified vertical piezoresponse of GaN at different polar facet (*c*-plane and *m*-plane). All samples were examined in a sealed chamber under a nitrogen atmosphere at 30 °C.

Fabrication of Nanometer-Thick Al_2O_3 Insulator Barrier: The Al_2O_3 insulators were synthesized on the *c*-plane and *m*-plane of the *p*-GaN film using ALD (Savannah G2 S200 PEALD). Different thicknesses of the insulator layer range from 0.95 to 4.78 nm were deposited precisely by controlling the ALD process. The key process parameters were as follows: pressure ≈0.37 Torr, temperature ≈120 °C, 90 sccm N_2 carrier gas, 0.015 s $cycle^{-1}$ H_2O, 0.1 s $cycle^{-1}$ trimethylgallium. As shown in Figure S2 (Supporting Information), the thicknesses of the Al_2O_3 insulating layers fabricated by 10, 20, 30, 40, and 50 cycles deposition were about 0.95, 1.91, 2.89, 3.85, and 4.78 nm, respectively.

Single Point Tunneling Measurements: The *I–V* curves of Pt/Al_2O_3/*p*-GaN tunneling junctions were measured using an Asylum Research Cypher ES AFM with ORCA mode (c-AFM). Conductive Pt/Ir-coated AFM tips with a radius of about 25 nm, spring constants ranged from 2.15 to 2.79 nN nm^{-1}, and a dual-gain ORCA module, were used to apply compressive force from about 0 to 850 nN and simultaneously measure the tunneling current. An electrical bias was applied through the substrate; this was swiped from 0 to 10 V at a ramping rate of about 0.8 V s^{-1}. The noise floor of the AFM system in these experiments is measured in Figure S3 (Supporting Information). The background noise was lower than ±10 and ±30 pA in 10 nA and 10 μA measurement range, respectively. All measurements were performed in a sealed chamber

under a nitrogen atmosphere at 30 °C controlled by the environmental control module in Asylum Research Cypher ES AFM.

Tactile Imaging Measurement: By modifying the "ScanMaster.ipf" program in Asylum Research Cypher ES AFM (provided by Asylum Research, Jason Li), the "Litho PFM" module was deployed to achieve spatial profile mapping of applied force, and at the same time, the current amplifier in ORCA module (conductive AFM, CAFM) was utilized to measure the corresponding current flow through the tunneling junctions simultaneously. The force distribution was mainly composed of very small force (≈18 nN, ≈9 MPa) and relatively large force (≈370 nN, ≈188 MPa). The very small force of about 18 nN was to ensure a good conductive contact without triggering the tunneling effect. And, the large force of about 370 nN was used to control the quantum tunneling while not destroying the insulator surface during 2D mechanical scanning process. Meanwhile, an electrical bias of 5.3 V was applied to provide the power. All measurements were performed in a sealed chamber under a nitrogen atmosphere at 30 °C.

Theoretical Calculations: The calculation was performed with COMSOL "*semiconductor module*" through a simple 1D model of 200 nm. The thickness of Al_2O_3 was from 0.5 to 15 nm, modeled as thin insulator gate with a relative dielectric constant of $\varepsilon_r = 5.7$ at left endpoint while the right endpoint was grounded. The GaN constants for numerical simulation were the relative dielectric constant $\varepsilon_r = 8.9$, the mobility of electrons $\mu_n = 1000\ cm^2\ V^{-1}\ s^{-1}$, and holes $\mu_p = 200\ cm^2\ V^{-1}\ s^{-1}$. The electron affinity χ adopted here was 4.1 eV and the band gap E_g was 3.39 eV. All the material coefficients above are available in COMSOL Multiphysics material library. The piezoelectric coefficient of GaN adopted here was $d_{33} = 12.8\ pm\ V^{-1}$.[39] The temperature was $T = 300$ K and the hole concentration was $N_A = 6 \times 10^{16}\ cm^{-3}$ given by the commercial sample. The piezotronic effect was considered with the assumption that the piezoelectric charge was distributed uniformly within a width of W_{piezo} as the previous literature demonstrated.[37] With these conditions applied, sweeps of voltage and strain were conducted using stationary solver with a finer physical-control mesh to demonstrate the potential distribution as shown in Figure 1c. Followed by a time-dependent study, capacitance–voltage results could be obtained as shown in Figure 1e. With the above results, current–voltage (*I*–*V*) could be given by Fowler–Nordheim tunneling formula[3]

$$J = \frac{q^2E^2}{16\pi^2\hbar\phi_{ox}}\exp\left(\frac{-4\sqrt{2m^*}(q\phi_{ox})^{3/2}}{3\hbar qE}\right) \quad (1)$$

where q is the electron charge, $\hbar$ is the reduced Planck constant, $m^* = 0.8m_0$ is the effective hole mass of GaN, ϕ_{ox} is the voltage drop across the oxide, and E is the corresponding mean electric field inside oxide.

Supporting Information

Supporting Information is available from the Wiley Online Library or from the author.

Acknowledgements

S.H.L., L.F.W., and X.L.F. contributed equally to this work. This research was supported by the National Key R&D Project from Minister of Science and Technology (2016YFA0202704), National Natural Science Foundation of China (nos. 51472111, 51432005, 5151101243, and 51561145021), and the National Program for Support of Top-notch Young Professionals.

Conflict of Interest

The authors declare no conflict of interest.

Keywords

mechanical gating, piezoelectric effect, piezotronic effect, quantum tunneling, tunneling junctions

Received: August 21, 2019
Revised: October 7, 2019
Published online:

[1] D. Griffiths, *Introduction to Quantum Mechanics*, Prentice Hall, New Jersey **2005**.
[2] S. M. Sze, K. K. Ng, *Physics of Semiconductor Devices*, 3rd ed., Wiley, New York **2006**.
[3] K. K. Thornber, T. C. McGill, C. A. Mead, *J. Appl. Phys.* **1967**, *38*, 2384.
[4] L. Esaki, *Phys. Rev.* **1958**, *109*, 603.
[5] I. Giaever, *Phys. Rev. Lett.* **1960**, *5*, 147.
[6] P. M. Tedrow, R. Meservey, *Phys. Rev. Lett.* **1971**, *26*, 192.
[7] M. Y. Zhuravlev, R. F. Sabirianov, S. S. Jaswal, E. Y. Tsymbal, *Phys. Rev. Lett.* **2005**, *94*, 246802.
[8] E. Y. Tsymbal, H. Kohlstedt, *Science* **2006**, *313*, 181.
[9] P. Maksymovych, S. Jesse, P. Yu, R. Ramesh, A. P. Baddorf, S. V. Kalinin, *Science* **2009**, *324*, 1421.
[10] W. G. Wang, M. Li, S. Hageman, C. L. Chien, *Nat. Mater.* **2012**, *11*, 64.
[11] D. Pantel, S. Goetze, D. Hesse, M. Alexe, *Nat. Mater.* **2012**, *11*, 289.
[12] A. A. Khajetoorians, B. Baxevanis, C. Hübner, T. Schlenk, S. Krause, T. O. Wehling, S. Lounis, A. Lichtenstein, D. Pfannkuche, J. Wiebe, R. Wiesendanger, *Science* **2013**, *339*, 55.
[13] V. Garcia, M. Bibes, L. Bocher, S. Valencia, F. Kronast, A. Crassous, X. Moya, S. Enouz-Vedrenne, A. Gloter, D. Imhoff, C. Deranlot, N. D. Mathur, S. Fusil, K. Bouzehouane, A. Barthélémy, *Science* **2010**, *327*, 1106.
[14] J. P. Eisenstein, L. N. Pfeiffer, K. W. West, *Phys. Rev. Lett.* **2017**, *118*, 186801.
[15] H. Ren, F. Pientka, S. Hart, A. T. Pierce, M. Kosowsky, L. Lunczer, R. Schlereth, B. Scharf, E. M. Hankiewicz, L. W. Molenkamp, B. I. Halperin, A. Yacoby, *Nature* **2019**, *569*, 93.
[16] A. Chen, Y. Wen, B. Fang, Y. Zhao, Q. Zhang, Y. Chang, P. Li, H. Wu, H. Huang, Y. Lu, Z. Zeng, J. Cai, X. Han, T. Wu, X. X. Zhang, Y. Zhao, *Nat. Commun.* **2019**, *10*, 243.
[17] L. L. Chang, E. E. Mendez, C. Tejedor, *Resonant Tunneling in Semiconductors: Physics and Applications*, Plenum Press, New York **1991**.
[18] F. B. Mancoff, N. D. Rizzo, B. N. Engel, S. Tehrani, *Nature* **2005**, *437*, 393.
[19] V. Garcia, S. Fusil, K. Bouzehouane, S. Enouz-Vedrenne, N. D. Mathur, A. Barthélémy, M. Bibes, *Nature* **2009**, *460*, 81.
[20] B. G. Park, J. Wunderlich, X. Martí, V. Holý, Y. Kurosaki, M. Yamada, H. Yamamoto, A. Nishide, J. Hayakawa, H. Takahashi, A. B. Shick, T. Jungwirth, *Nat. Mater.* **2011**, *10*, 347.
[21] A. Chanthbouala, A. Crassous, V. Garcia, K. Bouzehouane, S. Fusil, X. Moya, J. Allibe, B. Dlubak, J. Grollier, S. Xavier, C. Deranlot, A. Moshar, R. Proksch, N. D. Mathur, M. Bibes, A. Barthélémy, *Nat. Nanotechnol.* **2012**, *7*, 101.
[22] F. D. Natterer, K. Yang, W. Paul, P. Willke, T. Choi, T. Greber, A. J. Heinrich, C. P. Lutz, *Nature* **2017**, *543*, 226.
[23] Z. L. Wang, *Adv. Mater.* **2007**, *19*, 889.
[24] Z. L. Wang, *Nano Today* **2010**, *5*, 540.
[25] Z. L. Wang, W. Wu, *Natl. Sci. Rev.* **2014**, *1*, 62.
[26] W. Wu, Z. L. Wang, *Nat. Rev. Mater.* **2016**, *1*, 16031.
[27] W. Wu, L. Wang, Y. Li, F. Zhang, L. Lin, S. Niu, D. Chenet, X. Zhang, Y. Hao, T. F. Heinz, J. Hone, Z. L. Wang, *Nature* **2014**, *514*, 470.

[28] J. Qi, Y. W. Lan, A. Z. Stieg, J. H. Chen, Y. L. Zhong, L. J. Li, C. D. Chen, Y. Zhang, K. L. Wang, *Nat. Commun.* **2015**, *6*, 7430.
[29] L. Wang, S. Liu, G. Gao, Y. Pang, X. Yin, X. Feng, L. Zhu, Y. Bai, L. Chen, T. Xiao, X. D. Wang, Y. Qin, Z. L. Wang, *ACS Nano* **2018**, *12*, 4903.
[30] L. Wang, S. Liu, Z. Zhang, X. Feng, L. Zhu, H. Guo, W. Ding, L. Chen, Y. Qin, Z. L. Wang, *Nano Energy* **2019**, *60*, 724.
[31] C. Pan, L. Dong, G. Zhu, S. Niu, R. Yu, Q. Yang, Y. Liu, Z. L. Wang, *Nat. Photonics* **2013**, *7*, 752.
[32] S. Liu, L. Wang, X. Feng, Z. Wang, Q. Xu, S. Bai, Y. Qin, Z. L. Wang, *Adv. Mater.* **2017**, *29*, 1606346.
[33] R. Yu, X. Wang, W. Peng, W. Wu, Y. Ding, S. Li, Z. L. Wang, *ACS Nano* **2015**, *9*, 9822.
[34] W. Wu, Y. Wei, Z. L. Wang, *Adv. Mater.* **2010**, *22*, 4711.
[35] W. Wu, X. Wen, Z. L. Wang, *Science* **2013**, *340*, 952.
[36] H. Yuan, T. Lei, Y. Qin, R. Yang, *Nano Energy* **2019**, *59*, 84.
[37] Y. Zhang, Y. Liu, Z. L. Wang, *Adv. Mater.* **2011**, *23*, 3004.
[38] J. M. Wagner, F. Bechstedt, *Phys. Rev. B* **2002**, *66*, 115202.
[39] M. Minary-Jolandan, R. A. Bernal, I. Kujanishvili, V. Parpoil, H. D. Espinosa, *Nano Lett.* **2012**, *12*, 970.